

# Coherently excited nonlocal quantum features using polarization-frequency correlation between quantum erasers

Byoung S. Ham

School of Electrical Engineering and Computer Science, Gwangju Institute of Science and Technology

123 Chumcangwagi-ro, Buk-gu, Gwangju 61005, S. Korea

(Submitted on April 8, 2023, bham@gist.ac.kr)

## Abstract:

Photon indistinguishability is essential to understanding “mysterious” quantum features from the viewpoint of the wave-particle duality in quantum mechanics. The fundamental physics of indistinguishability lies in the quantum superposition of orthonormal bases of a single photon such as in a quantum eraser. Here, a pure coherence approach is applied for coherently excited nonlocal correlation using polarization-frequency correlation of Poisson-distributed coherent photon pairs. For this, a heterodyne detection technique is adopted for coincidence measurements in a delayed-choice quantum eraser scheme, resulting in an entangled photon pair-like inseparable basis product. The role of coincidence detection is investigated for the selective measurement-based quantum features, where coherence between paired photons is the bedrock of the quantum correlation. Finally, the Bell inequality violation is numerically demonstrated for the analytically derived coherence solutions.

## Introduction

In quantum mechanics, measurements can retrospectively affect the original quantum state [1,2]. Such measurement-based quantum mechanics has been intensively studied for various delayed-choice experiments over the last several decades [3-12]. Not only a single photon-based quantum superposition [4-7] but also two photon-based quantum entanglements [10-13] has been intensively studied for the mysterious quantum feature violating the causality of classical physics. Potential quantum loopholes in such a quantum system have already been closed for detection [13,16], locality [14], sampling [13,15,16], and free will [17] parameters. The nonlocal correlation between space-like separated photons results in a violation of local realism in quantum mechanics [18-24]. Classical realism is for predetermined physical laws that are not influenced by the nonlocal action of measurements as claimed by Einstein and his colleagues [18]. Nonlocal realism defies classical reality via the so-called “spooky action at a distance” [20]. However, this nonlocal correlation violating local realism has not been clearly understood yet. To satisfy nonlocal correlation, it is commonly accepted that measured photons must be nonclassical [13-23].

Here, a contradictory idea of nonlocal correlation is presented by classical means of coherence optics. For this, a coherently excited Franson-type-like nonlocal correlation is proposed for the inseparable basis-product relation of local parameters between quantum erasers. Here, the Franson-type-like means a noninterfering Mach-Zehnder interferometer (NMZI). For the quantum feature analysis, a pair of coherent photons is manipulated to be frequency-polarization correlated by synchronized acousto-optic modulators (AOMs), whose output photon pairs are coincidentally measured via a heterodyne detection technique. Unlike common coherence optics, however, the present coherent scheme still belongs to a microscopic regime of a single photon for measurements. Thus, the goal of the present paper is to show the role of quantum measurements in the generation process of nonlocal correlation. For heterodyne detection, the temporal resolution of a single photon detector must be better than the inverse of the bandwidth of AOMs.

Over the last few decades, the quantum feature of Franson-type nonlocal correlation [24] has been experimentally demonstrated for the violation of local realism [25-30]. Recently, the Franson correlation has been coherently investigated for the role of coincidence measurements [31]. In that study, a common inseparable basis-product relation is interpreted for selective measurements in a usual coincidence detection manner, resulting in the second-order quantum superposition [31]. Wheeler’s delayed-choice experiments [3-12] have also been newly interpreted for the post-measurement control of polarization basis using a pure coherence approach, resulting in the same causality violation even in a macroscopic regime [32]. Unlike the Franson correlation [24-30], the delayed

choice relates to the first-order quantum superposition of a single photon in an interferometric system [2-4]. The coherent photon-excited inseparable basis products [32] have also been investigated in a delayed-choice quantum eraser, where the coherent photons are manipulated for frequency-polarization correlation using a pair of AOMs [33].

## Results

### Coherently excited polarization-frequency correlation

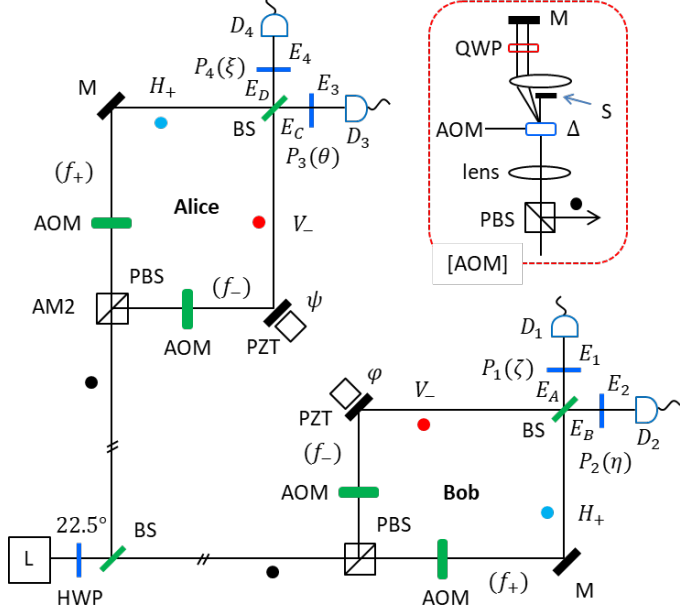


Fig. 1. Schematic of coherently excited nonlocal correlation in a quantum eraser scheme. AOM: acousto-optic modulator, BS: beam splitter, D: single photon detector, H (V): horizontal (vertical) polarization, HWP: half-wave plate, L: laser, M: mirror, P: polarizer, PBS: polarizing BS, PZT: piezo-electric transducer, QWP: quarter-wave plate. The black, blue, and red dots indicate a single photon.  $f_-$  ( $f_+$ ) represents  $-\delta f$  ( $+\delta f$ ) detuned frequency from the center frequency  $f_0$  by AOMs. The Inset is for AOM's double-pass scheme.

Figure 1 shows a schematic of the coherently excited Franson-type-like nonlocal correlation in a quantum eraser scheme. For this, a synchronized pair of double-pass AOMs is used for oppositely detuned frequency manipulation, resulting in polarization-frequency correlation, i.e.,  $f_+ - H_+$  and  $f_- - V_-$  relationship. For random orthogonal polarization bases, a 22.5°-rotated half-wave plate (HWP) is placed right after the attenuated laser. Each set of polarization-frequency correlated photons is locally controlled by Alice and Bob independently. For the mutual coherence between paired photons, AOM pairs are synchronized. To satisfy the nonlocal condition, the distance between the first BS and polarizers is set to be space-like separated, where the light cone should violate causality. In each party, the NMZI output photon's polarizations are random on the second BS. Due to orthogonal polarization bases, each NMZI results in no fringe in the output intensities by Fresnel-Arago law [34]. By adding a polarizer in each output path, however, a quantum eraser scheme is satisfied for the wave-particle duality, resulting in fringes [3,4]. For an arbitrary angle of Ps, a common polarization basis is chosen for the coherence (indistinguishability) of orthogonally polarized photons. Due to the independence between polarizers, any violation of the causality witnesses the “delayed choice” of quantum mechanics [3-13].

Regarding the light source L in Fig. 1, the mean photon number is set to be extremely low, satisfying the incoherence condition between consecutive single photons. For this, a mean consecutive photon distance is set to be much longer than the laser's coherence length. For the coincidence measurements, however, only Poisson-

distributed doubly bunched photons are post-selected for the nonlocal feature at  $\sim 1\%$  ratio of single photons [35]. Unlike SPDC-based entangled photons, whose frequencies are oppositely detuned across the center frequency  $f_0$ , coherent photons from L have no such detuning relation due to the cavity optics. The purpose of AOMs is to generate such a SPDC-like symmetric frequency relation in each NMZI. For this, the laser linewidth must be much narrower than the bandwidth of AOMs. In Fig. 1, a doubly bunched photon pair can be either split into both NMZIs or bunched together into one NMZI by the first BS at an equal chance. The bunched case is automatically dropped out by the definition of coincidence measurements between two NMZIs. For the split case, however, the NMZI output photon can be either vertical or horizontal at an equal chance, where the blue and red dots in Fig. 1 represent the probability amplitudes of a single photon (black dot). The goal of heterodyne detection is to selectively choose orthogonally polarized photon pairs only between two parties. Thus, the success rate of the heterodyne detection-based coincidence measurements is one out of four for a given photon pair to two sets of detectors (see Section A of the Supplementary Materials). All other cases are simply excluded without affecting results.

### Analysis

For the coherence approach in Fig. 1, each photon's amplitude is represented by  $E_0$ . Each photon pair has the wave nature at a monochromatic frequency  $f_j$ , where  $f_j = f_0 \pm \delta f_j$ . The AOM-generated photons should show an ensemble feature with effective-coherence length  $l_c = c\Delta^{-1}$ , where  $c$  is the speed of light and  $\Delta$  is the AOM's bandwidth. As shown in the Inset, the AOM is set for a double-pass scheme for  $\delta f_j$ -independent propagation direction. By coincidence detection, only doubly-bunched photons are selectively chosen from the attenuated laser [35]. In this case, 50 % of non-split (bunched) photons by the first BS are discarded by coincidence detection. A heterodyne detection method is adopted to conditionally exclude the same polarization basis between NMZI output photons for coincidence measurements of split photons, allowing only opposite-basis products.

According to synchronized AOMs, the post-selected output photons from both NMZIs via heterodyne detection-based coincidence measurements can be represented as:

$$\begin{bmatrix} E_A^j \\ E_B^j \end{bmatrix} = \frac{E_0}{\sqrt{2}} e^{i\alpha} e^{i(k_0 r - \omega_0 t)} \begin{bmatrix} H_+ e^{i\delta f_j t_+} - V_- e^{-i\delta f_j t_-} \\ i(H_+ e^{i\delta f_j t_+} + V_- e^{-i\delta f_j t_-}) \end{bmatrix}, \quad (1)$$

$$\begin{bmatrix} E_C^j \\ E_D^j \end{bmatrix} = \frac{E_0}{\sqrt{2}} e^{i(k_0 r - \omega_0 t)} \begin{bmatrix} H_+ e^{i\delta f_j t_+} - V_- e^{-i\delta f_j t_-} \\ i(H_+ e^{i\delta f_j t_+} - V_- e^{-i\delta f_j t_-}) \end{bmatrix}, \quad (2)$$

where  $H_{\pm}$  and  $V_{\pm}$  denote unit vectors of horizontal and vertical polarizations, respectively. These polarized photons are correlated to the frequencies  $f_{\pm}$  by AOMs. The global phase  $e^{i\alpha}$  in Eq. (1) is due to the arbitrary path-length difference from the first BS to both NMZIs. Equations (1) and (2) are for the first-order amplitudes of a single photon in each NMZI, resulting in no fringes due to PBS, satisfying distinguishable photon characteristics.

For the polarizer-induced quantum eraser, Eqs. (1) and (2) are rewritten as:

$$\begin{bmatrix} E_1^j \\ E_2^j \end{bmatrix} = \frac{E_0}{\sqrt{2}} e^{i\eta} e^{i(k_0 r - \omega_0 t)} e^{i\delta f_j t_+} \begin{bmatrix} H_+ \cos\zeta - V_- \sin\zeta e^{-i\varphi_j} \\ i(H_+ \cos\eta + V_- \sin\eta e^{-i\varphi_j}) \end{bmatrix}, \quad (3)$$

$$\begin{bmatrix} E_3^j \\ E_4^j \end{bmatrix} = \frac{E_0}{\sqrt{2}} e^{i(k_0 r - \omega_0 t)} e^{i\delta f_j t_+} \begin{bmatrix} H_+ \cos\theta - V_- \sin\theta e^{-i\psi_j} \\ i(H_+ \cos\xi + V_- \sin\xi e^{-i\psi_j}) \end{bmatrix}, \quad (4)$$

where  $\zeta$ ,  $\eta$ ,  $\theta$ , and  $\xi$  are the rotation angles of each polarizer from the horizontal axis to the counter-clockwise direction. Due to the same polarization projection of the orthogonally polarized photons onto the corresponding polarizer in each equation, the originally non-interacting photons become interfered: a quantum eraser. Regarding the AOM-induced detuning  $\pm\delta f_j$  across the center frequency  $f_0$ , the phase can be expressed by  $\varphi_j = 2\delta f_j \tau_B$  and  $\psi_j = 2\delta f_j \tau_A$ , where  $\tau_k$  ( $k = A; B$ ) is the time delay between NMZI paths.

The corresponding intensities of the paired  $j^{\text{th}}$  photons are as follows:

$$\begin{aligned} I_1^j &= \frac{I_0}{2} (H_+ \cos\zeta - V_- \sin\zeta e^{-i\varphi_j}) (H_+ \cos\zeta - V_- \sin\zeta e^{i\varphi_j}) \\ &= \frac{I_0}{2} (1 - \sin 2\zeta \cos \varphi_j), \end{aligned} \quad (5)$$

$$I_2^j = \frac{I_0}{2} (H_+ \cos \eta + V_- \sin \eta e^{-i\varphi_j}) (H_+ \cos \eta + V_- \sin \eta e^{i\varphi_j}) \\ = \frac{I_0}{2} (1 + \sin 2\eta \cos \varphi_j), \quad (6)$$

$$I_3^j = \frac{I_0}{2} (H_+ \cos \theta - V_- \sin \theta e^{-i\psi_j}) (H_+ \cos \theta - V_- \sin \theta e^{i\psi_j}) \\ = \frac{I_0}{2} (1 - \sin 2\theta \cos \psi_j), \quad (7)$$

$$I_4^j = \frac{I_0}{2} (H_+ \cos \xi + V_- \sin \xi e^{-i\psi_j}) (H_+ \cos \xi + V_- \sin \xi e^{i\psi_j}) \\ = \frac{I_0}{2} (1 + \sin 2\xi \cos \psi_j). \quad (8)$$

From Eqs. (5)-(8), each local measurement of the  $j^{\text{th}}$  photon shows interference fringes with a decoherence factor  $\cos \varphi_j$  or  $\cos \psi_j$ . In each NMZI, such a phenomenon is called a quantum eraser which has been observed in both SPDC- and single-photon cases [9]. For an ensemble,  $\frac{1}{N} \sum_j I_k^j = \frac{\langle I_0 \rangle}{2N} \langle \sum_j (1 \pm \sin 2\rho \cos \chi_j) \rangle$  is considered for  $\tau_A = \tau_B \sim 0$ , where  $k=1 \sim 4$ ,  $\rho = \zeta, \eta, \theta, \xi$ , and  $\chi = \varphi, \psi$ . As the  $\chi_j$  range increases, the fringe visibility decreases (see Section B of the Supplementary Material). If  $\tau_A \gg \Delta^{-1}$ , no fringe exists, resulting in  $\langle I_k \rangle = \frac{\langle I_0 \rangle}{2}$ . Thus, the function of the polarizers for the quantum eraser is successfully demonstrated for the individual coherence retrievals in NMZIs of Fig. 1.

For the nonlocal correlation, coincidence detection is analyzed for the pair of local detectors  $D_1$  and  $D_4$  between space-like separated two parties:

$$R_{14}^j = \frac{I_0^2}{4} (H_+ \cos \zeta - V_- \sin \zeta e^{-i\varphi_j}) (H_+ \cos \xi + V_- \sin \xi e^{-i\psi_j}) (cc). \quad (9)$$

The corresponding mean value  $\langle R_{14}(\tau) \rangle (\equiv \frac{1}{N} \sum_{j=1}^N R_{14}^j(\tau))$  of Eq. (9) results in nonlocal correlation via the heterodyne detection-based coincident measurements:

$$\langle R_{14}(\tau) \rangle = \frac{\langle I_0^2 \rangle}{4} H_+ V_- \langle (-\sin \zeta \cos \xi e^{-i\varphi_j} + \cos \zeta \sin \xi e^{-i\psi_j}) (c.c.) \rangle, \\ = \frac{\langle I_0^2 \rangle}{4} \langle \sin^2(\zeta - \xi) + 2 \sin \zeta \cos \xi \cos \zeta \sin \xi (1 - \cos(\psi_j - \varphi_j)) \rangle, \quad (10)$$

where  $\tau = \tau_A - \tau_B$ . For the coincidence detection, i.e.,  $\tau_A = \tau_B$ ,  $\langle R_{14}(0) \rangle = \frac{\langle I_0^2 \rangle}{4} \sin^2(\zeta - \xi)$  is satisfied for the joint parameter relation of local polarizers. This expression is the quintessence of the nonlocal quantum feature [23]. As the time delay  $\tau$  increases in the order of  $\Delta^{-1}$ , the deterioration of the nonlocal feature increases, too. For  $\tau \gg \Delta^{-1}$ , Eq. (10) turns out to be classical (discussed below). Likewise,  $\langle R_{23}(0) \rangle = \langle R_{14}(0) \rangle$  is satisfied.

Similarly, the following correlation relation is obtained between detectors  $D_1$  and  $D_3$  (see Section C of the Supplementary Material):

$$\langle R_{13}(0) \rangle = \langle R_{24}(0) \rangle = \frac{\langle I_0^2 \rangle}{4} \sin^2(\zeta + \theta), \quad (11)$$

where Eq. (11) is opposite to Eq. (10) in the fringe pattern (see Fig. 2). The sum of  $\langle R_{14}(0) \rangle$  and  $\langle R_{13}(0) \rangle$  ( $\langle R_{23}(0) \rangle$  and  $\langle R_{24}(0) \rangle$ ) shows the classical feature without the joint parameter relation, which is equal to  $R_{14}(\tau \gg \Delta^{-1})$  (see Section C of the Supplementary Material and Fig. 3). Thus, the coherently excited nonlocal quantum correlation is successfully derived for Fig. 1 via polarization-frequency correlation and heterodyne detection-based coincidence measurements.

Figure 2 shows numerical calculations of the analytical solutions in Eqs. (5)-(11). The upper panels are for the quantum features of Bell inequality violation at  $\tau = 0$ , i.e.,  $\psi_j = \varphi_j$ . As shown in the upper right panel, coincidence detection-based two-photon correlation coefficients are calculated from the four points. As a result,  $E(\alpha, \beta) = [R_{14}(\alpha, \beta) + R_{23}(\alpha, \beta) - R_{13}(\alpha, \beta) - R_{24}(\alpha, \beta)] = 0$  is obtained from the left lower point of the blue ( $R_{14}$ ) and red ( $R_{14}$ ) dotted curves, where  $\alpha = \zeta, \eta$  and  $\beta = \xi, \theta$  [23,37]. Using those calculated  $E$  values for  $(\alpha, \alpha', \beta, \beta') = (0^\circ, 45^\circ, 22.5^\circ, 67.5^\circ)$ , the Bell parameter  $S$  is calculated for the violation of local hidden variable theory bound by  $S=2$  (see Section D of the Supplementary Materials):  $S(\alpha, \alpha', \beta, \beta') = \left| E(\alpha, \beta) + E(\alpha', \beta) - E(\alpha, \beta') + E(\alpha', \beta') \right| = 2\sqrt{2}$ .

On the contrary to the upper panels for the quantum features obtained by the heterodyne detection-based coincidence measurements, the lower panels of Fig. 2 are the corresponding classical features. For this, both locally measured intensity products,  $I_1I_4$  ( $= I_2I_3$ ) and  $I_1I_3$  ( $= I_2I_4$ ) are calculated for  $E$  values, where  $I_1I_4$  and  $I_1I_3$  are represented by blue and red curves in the lower right panel, respectively. Each curve is for  $(\xi, \theta) = (22.5^\circ, 67.5^\circ)$ . Unlike the upper right panel, the Bell parameter  $S$  of the lower right panel does not violate the classical upper bound:  $S=0$  (see Section E of the Supplementary Materials). Thus, the present coherence approach is successful to excite the nonlocal quantum feature of Bell inequality violation, where the joint-parameter relations in Eqs. (10) and (11) are the origin of the so-called quantum steering [36]. However, it is quite interesting that Eqs. (10) and (11) are seemingly contradictory to the violation of local realism simply because the paired photons are coherent to preserve their predetermined realism no matter how far they are apart within  $\tau < \Delta^{-1}$ , if a correct understanding of the coincidence detection is lacked.

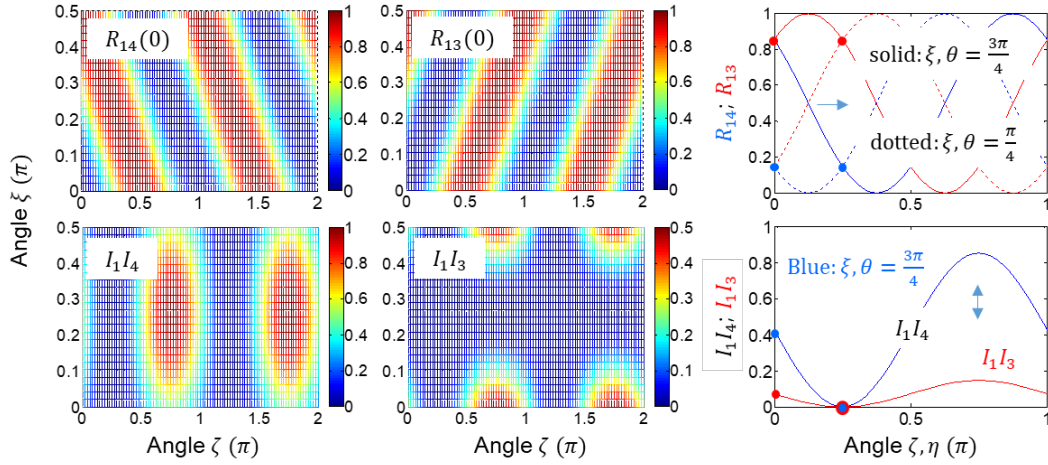


Fig. 2. Numerical calculations for Fig. 1. (Upper panels) Nonlocal quantum feature of Eqs. (10) and (11) for  $\tau = 0$ . (Lower panels) Intensity product of  $I_1I_4$ ;  $I_1I_3$ . (Right-end column) Blue:  $R_{14}$  ( $= R_{23}$ );  $I_1I_4$  ( $= I_2I_3$ ). Red:  $R_{13}$  ( $= R_{24}$ );  $I_1I_3$  ( $= I_2I_4$ )

Figure 3 shows the deterioration of the quantum feature as the time delay increases. At  $\tau \gg \Delta^{-1}$ , the nonlocal quantum feature completely disappears, resulting in a classical feature without satisfying the joint parameter relation. Compared with the local intensity product  $I_1I_4$  ( $\neq I_1I_4$ ) in Fig. 2, Fig. 3 shows a bit different feature, where  $R_{13} = R_{14}$  at  $\tau \gg \Delta^{-1}$ . The Bell parameter  $S$  does not violate the Bell inequality condition, either (see Section F of the Supplementary Materials):  $S=0$ . Thus, the bedrock of the nonlocal quantum correlation is the mutual coherence between paired photons via coincidence measurements.

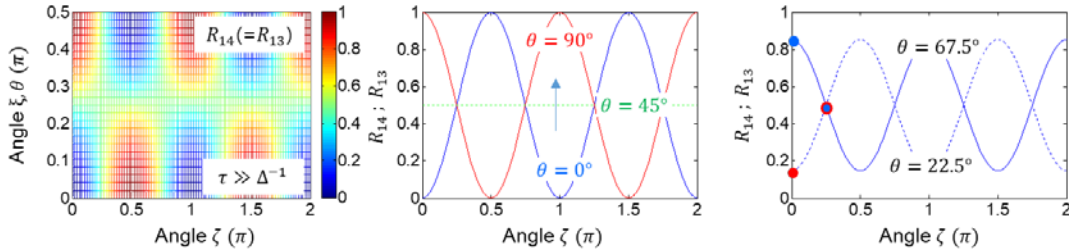


Fig. 3. Numerical calculations for Eq. (10) and (11) at  $\tau \gg \Delta^{-1}$ .  $\xi = \theta$  is satisfied independently for  $\zeta$ .

## Discussion

Does the nonlocal quantum feature in Eqs. (10) and (11) violate local realism, i.e., the hidden variable theory [18-20]? The heart of local realism is the pre-determinism by classical laws. Thus, local realism states that any action in one party cannot influence the physical entity in the other party apart by a space-like separation. The quantum feature derived in Eq. (10) requires mutual coherence between paired photons for measurement modified basis products, as demonstrated in Figs. 2 and 3. Within this coherence, the joint-parameter relation confirms that local action in one party affects measurements in the other party, as demonstrated in the upper right panel of Fig. 2. Not until measured by coincidence detection, however, no one knows the result yet. As the retrieval of the predetermined coherence feature is the essence of the quantum eraser, the coincidence measurement between paired photons is just for a check-up process of the preexisting correlation in a specific way. In other words, the key to the quantum correlation is not the space-like separation but the mutual coherence check-up process via a measurement modification. Thus, the nonlocal realism is for predetermined correlation rooted in mutual coherence via a coincidence detection-caused measurement modification process.

## Conclusion

Using coherence manipulations of polarization-frequency correlation in NMZIs for a quantum eraser, the nonlocal correlation between space-like separated NMZI output photons was analyzed and numerically demonstrated for the Bell inequality violation. The manipulation of polarization-frequency correlation was conducted by a pair of synchronized AOMs in both NMZIs. The role of heterodyne detection is to selectively choose orthogonal polarization-basis products only, resulting in quantum features in a joint-parameter relation. Unlike the conventional understanding of the nonlocal correlation limited to quantum particles such as entangled photon pairs, the present coherence approach using an attenuated laser was contradictory to the common understanding that nonlocal correlation could not be achieved by any classical means. With heterodyne detection-caused measurement-basis modifications, however, the proposed coherence scheme was successful for coherently excited nonlocal quantum features in a space-like separation regime, satisfying Bell inequality violation. The coherence solutions of the nonlocal quantum feature between NMZIs were also numerically discussed for the coherence-based quantum feature, where effective coherence between paired photons was the bedrock.

## Acknowledgments

This work was supported by the ICT R&D program of MSIT/IITP (2023-2021-0-01810), the development of elemental technologies for an ultrasecure quantum internet. BSH also acknowledges that this work was supported by the GIST Research Project in 2023.

## Reference

1. Bohr, N. in *Quantum Theory and Measurement*, Wheeler, J.A. & Zurek, W.H. Eds. (Princeton Univ. Press, Princeton, NJ), pages 949, 1984.
2. Wheeler, J. A. in *Quantum Theory and Measurement*, J. A. Wheeler and W. H. Zurek eds (Princeton University Press, 1984), pp. 182-213.
3. Scully, M. O., Englert, B.-G. & Walther, H. Quantum optical tests of complementarity, *Nature* **351**, 111-116 (1991).
4. Jacques, V., Wu, E., Grosshans, F., Treussart, F., Grangier, P., Aspect, A. & Roch, J.-F. Experimental realization of Wheeler's delayed-choice Gedanken Experiment. *Science* **315**, 966-978 (2007).
5. Manning, A. G., Khakimov, R. I., Dall, R. G. & Truscott, A. G. Wheeler's delayed-choice gedanken experiment with a single atom. *Nature Phys.* **11**, 539-542 (2015).
6. Aharonov, Y. & Zubairy, M. S. Time and the Quantum: Erasing the Past and Impacting the Future. *Science* **307**, 875-879 (2005).
7. Tang, J.-S., Li, Y.-L., Xu, X.-Y., Xiang, G.-Y., Li, C.-F. & Guo, G.-C. Realization of quantum Wheeler's delayed-choice experiment. *Nature Photon.* **6**, 600-604 (2012).
8. Ionicioiu, R. & Terno, D. R. Proposal for a Quantum Delayed-Choice Experiment. *Phys. Rev. Lett.* **107**, 230406 (2011).

9. Ma, X.-S., Kofler, J. & Zeilinger, A. Delayed-choice gedanken experiments and their realizations. *Rev. Mod. Phys.* **88**, 015005 (2016).
10. Herzog, T. J., Kwiat, P. G., Weinfurter, H. & Zeilinger, A. Complementarity and the quantum eraser. *Phys. Rev. Lett.* **75**, 3034-3037 (1995).
11. Ionicioiu, R., Jennewein, T., Mann, R. B. & Terno, D. R. Is wave-particle objectivity compatible with determinism and locality? *Nature Communi.* **5**, 4997 (2014).
12. Wang, K., Xu, Q., Zhu, S. & Ma, X.-S. Quantum wave-particle superposition in a delayed-choice experiment. *Nature Photon.* **13**, 872-877 (2019).
13. Christensen, B. G. *et al.*, Detection-loophole-free test of quantum nonlocality, and applications. *Phys. Rev. Lett.* **111**, 130406 (2013).
14. Aspect, A. Closing the door on Einstein and Bohr's quantum debate. *Physics* **8**, 123 (2015).
15. Giustina, M. *et al.*, Significant-loophole-free test of Bell's theorem with entangled photons. *Phys. Rev. Lett.* **115**, 250401 (2015).
16. Hensen, B. *et al.*, Loophole-free Bell inequality violation using electron spins separated by 1.3 kilometres. *Nature* **526**, 682-686 (2015).
17. Abellan, C. *et al.*, Challenging local realism with human choices. *Nature* **557**, 212-216 (2018).
18. Einstein, A., Podolsky, B. & Rosen, N. Can quantum-mechanical description of physical reality be considered complete? *Phys. Rev.* **47**, 777-780 (1935).
19. Wiseman, H., Death by experiment for local realism. *Nature* **526**, 649-650 (2015).
20. Bell, J. S. On the Einstein Podolsky Rosen paradox. *Physics* **1**, 195-200 (1964).
21. Clauser, J. F., Horne, M. A., Shimony, A. & Holt, R. A. Proposed experiment to test local hidden-variable theories. *Phys. Rev. Lett.* **23**, 880-884 (1969).
22. Aspect, A., Grangier, P. & Roger, G. Experimental realization of Einstein-Podolsky-Rosen-Bohm Gedankenexperiment: A new violation of Bell's inequalities. *Phys. Rev. Lett.* **49**, 91-94 (1982).
23. Weihs, G., Jennewein, T., Simon, C., Weinfurter, H. & Zeilinger, A. Violation of Bell's inequality under strict Einstein locality. *Phys. Rev. Lett.* **81**, 5039-5042 (1998).
24. Franson, J. D. Bell inequality for position and time. *Phys. Rev. Lett.* **62**, 2205-2208 (1989).
25. Kwiat, P. G., Steinberg, A. M. & Chiao, R. Y. High-visibility interference in a Bell-inequality experiment for energy and time. *Phys. Rev. A* **47**, R2472-R2475 (1993).
26. Lima, G., Vallone, G., Chiuri, A., Cabello, A. & Mataloni, P. Experimental Bell-inequality violation without the postselection loophole. *Phys. Rev. A* **81**, 040101(R) (2010).
27. Carvacho, G. *et al.*, Postselection-loophole-free Bell test over an installed optical fiber network. *Phys. Rev. Lett.* **115**, 030503 (2015).
28. Marcikic, I., de Riedmatten, H., Tittel, W., Scarani, V., Zbinden, H. & Gisin, N. Time-bin entangled qubits for quantum communication created by femtosecond pulses. *Phys. Rev. A* **66**, 062308 (2002).
29. Aerts, S., Kwiat, P., Larsson, J.-Å. & Żukowski, M. Two-photon Franson-type experiments and local realism. *Phys. Rev. Lett.* **83**, 2872-2875 (1999).
30. Cuevas, A. *et al.*, Long-distance distribution of genuine energy-time entanglement. *Nature Communi.* **4**, 2871 (2013).
31. Ham, B. S. The origin of Franson-type nonlocal correlation. arXiv:2112.10148 (2023).
32. Ham, B. S. A coherence interpretation of nonlocal realism in the delayed-choice quantum eraser. arXiv:2302.13474 (2023).
33. Ham, B. S. Coherently driven quantum features using a linear optics-based polarization-basis control. arXiv:2303.12628 (2023).
34. Henry, M. Fresnel-Arago laws for interference in polarized light: A demonstration experiment. *Am. J. Phys.* **49**, 690 (1981).
35. Kim, S. and Ham, B. S. Revisiting self-interference in Young's double-slit experiments. *Sci. Rep.* **13**, 977 (2023).
36. Uola, R., Costa, A. C. S., Nguyen, H. C. & Gühne, O. Quantum steering. *Rev. Mod. Phys.* **92**, 015001 (2020).

37. Clauser, J. F., Horne, M. A., Shimony, A. & Holt, R. A. Proposed experiment to test local hidden-variable theories. *Phys. Rev. Lett.* **23**, 880–884 (1969).

**Author contributions** B.S.H. conceived the idea and wrote the manuscript.

**Correspondence and request of materials** should be addressed to BSH (email: bham@gist.ac.kr).

**Competing interests** The author declares no competing interests.